Contents lists available at AccScience Publishing
Nonlinear Science and Control Engineering (NSCE)
Vol. 2, No. 1 (2026)
https://accscience.com/journal/nsce

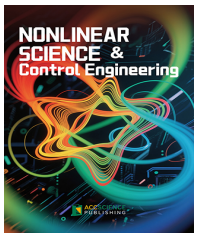

Parametric analysis and statistical characterization of extreme events in a minimal Lorenz-like chaotic system

Jianning Huang[1*], Paul Didier Kamdem Kuate[2], and Achille Ecladore Tchahou Tchendjeu[3]

[1]*School of Mathematics and Information Science, Nanchang Normal University, Nanchang, Jiangxi, China*
[2]*Department of Electrical and Power Engineering, Higher Technical Teachers Training College, University of Bamenda, Bambili, Northwest Region, Cameroon*
[3]*Department of Electrical and Electronic Engineering, National Polytechnic Institute, University of Bamenda, Bambili, Northwest Region, Cameroon*

Article History:
Received: November 3, 2025
Revised: November 28, 2025
Accepted: December 5, 2025
Published online: December 24, 2025

ABSTRACT

Extreme events are rare, high-impact phenomena that deviate significantly from nominal behavior, posing significant challenges across both natural and engineered systems, from climate dynamics to neurological conditions. The present study investigates the intricate dynamics and emergence of extreme events in a minimal, nonhyperbolic Lorenz-like chaotic system, characterized by piecewise linear nonlinearities. By leveraging standard nonlinear analysis and statistical tools, we explore how the system parameters govern its dynamical transitions, amplitude control, and propensity for extreme events. For small values of the control parameter, the system exhibits chaotic behavior, characterized by frequent, high-amplitude excursions indicative of extreme events. Statistical analyses of local maxima and inter-event intervals further characterize these events, highlighting their rarity and high magnitude through heavy-tailed probability distributions. The simplicity and controllability of the proposed model make it a valuable tool for theoretical exploration and practical applications in fields such as climate modeling, engineering, and nonlinear dynamics.

Keywords: Amplitude control; Chaotic dynamics; Extreme events; Nonhyperbolic system; Parametric control; Piecewise linear nonlinearity

1. Introduction

Investigations into extreme events—rare, high-impact occurrences that deviate from a system's canonical behavior—have recently received increased attention. Such phenomena can be observed in a variety of natural and engineered systems, ranging from abrupt, drastic climate changes to sudden, abnormal neurological conditions.[1–4] Whether manifesting as catastrophic market crashes, unprecedented weather phenomena, or sudden ecological

***Corresponding author**:
Jianning Huang (huangjianning@ncnu.edu.cn).

Citation:
Huang J, Kuate PDK, Tchendjeu AET. Parametric analysis and statistical characterization of extreme events in a minimal Lorenz-like chaotic system. *Nonlinear Sci Cont Eng.* 2026;2(1):025450017. doi: 10.36922/NSCE025450017

shifts, these events pose significant threats to human society. Extreme weather events, such as hurricanes, intense heat waves, prolonged droughts, and torrential rain, are often cited as typical examples due to their particularly destructive power and social impact.[5–7] In the contemporary scientific paradigm, these events are no longer regarded as mere random abnormalities. Instead, they are recognized as consequences of intricate and nonlinear interactions within the underlying mechanisms governing a convoluted climatic system.[8,9] This inherent complexity renders them remarkably challenging to predict. However, the study of these phenomena is not limited to theoretical models or climate systems but is also critical for the safety and reliability of complex systems such as mechanical structures subject to nonlinear impacts.[10]

The theoretical underpinnings of this paradigm can be traced back to the seminal research contributions of the meteorologist Lorenz in the early 1960s.[11] In the course of simulating a highly simplified model of atmospheric convection, he made a crucial discovery as follows: his deterministic model, composed of only three differential equations, could produce an apparently random and non-repeatable trajectory, which he described as chaotic.[11–13] This pioneering work established the notion of sensitive dependence on initial conditions (ICs), now recognized as the butterfly effect, demonstrating that even an imperceptible alteration in the initial state of a system could lead to unexpected long-term dynamic behavior. A major aspect of this discovery resides in the capability of very simple rules to generate highly complex dynamical behavior. Dependence on ICs makes long-term weather forecasting difficult and highlights the challenges posed by predicting extreme and destructive climate phenomena.[14]

Building on Lorenz's groundbreaking work, a considerable body of research has proposed simplified mathematical models that retain the essence of chaotic dynamics while avoiding the intricacies inherent to large-scale climate models.[15–17] These studies commonly adopt a high level of abstraction by isolating key parameters and nonlinear mechanisms capable of triggering the emergence of complex behaviors. A notable example of this approach is the physically motivated diffusionless Lorenz equations (DLEs) proposed by van der Schrier and Maas[18] and Dong,[19] which feature only five terms, including a pair of cross-product nonlinearities, and a single parameter. In the framework of elegant chaos, Sprott[20–22] demonstrated, using a palette of 19 (A–S) examples of simple mathematical models, that chaotic dynamics can occur in low-dimensional autonomous nonlinear systems simpler than the original Lorenz equations. It has been demonstrated that the Sprott-B and Sprott-C systems, which feature only five terms and two nonlinearities, similar to the DLE, also exhibit a Lorenz-like butterfly chaotic attractor.[23] Following this parsimonious modeling framework, Kamdem Kuate et al.[24] introduced a three-dimensional chaotic system that retained the core feedback loops of the original Lorenz equations while replacing nonlinear terms with simple piecewise linear (PWL) functions. This equation design renders the model amenable to rigorous dynamic analysis, allowing for simple identification of bifurcations and easier parametric exploration of chaotic regimes. In contrast to the smooth nonlinearities of the Lorenz system, sharp transitions in PWL functions have been shown to engender distinct and well-defined boundaries in phase space, thereby fragmenting the system dynamics across different linear regions.[25–27] However, the transitions between these regions are recognized to induce highly complex dynamic behaviors, including chaos, multistability, spikes, and multiscroll attractors.[28–31]

The model under consideration is governed by only two parameters: the bifurcation parameter, which controls transitions between different operating regimes, and the amplitude controller, which adjusts the attractor size. This minimal design in system dimension, nonlinearities, and parametric space not only serves as a key advantage for analyzing and investigating the mechanisms underlying chaos and extreme events but also makes the model an ideal pedagogical tool and a valuable testbed for developing characterization techniques that can be generalized to complex systems. The contributions of the present study are as follows:

(i) A comprehensive dynamic analysis of a highly simplified Lorenz-like system was conducted. Precisely, mapping its phase space and identifying the conditions under which chaotic behavior and extreme events emerged.

(ii) The effect of each parameter on the magnitude and dynamics of this minimal chaotic system was investigated in both time and frequency domains, with the aim of identifying the state variables that support the dynamical complexity.

(iii) Finally, the occurrence of extreme events in the proposed simplified model was investigated, demonstrating that such intricate and dynamical behavior can also manifest in small systems, described by simple equations and evolution rules.

The remainder of this paper is organized as follows: **Section 2** provides a comprehensive overview of the nonhyperbolic Lorenz-like system under consideration and characterizes its equilibrium. **Section 3** focuses on parametric analyses and explores the variety of dynamic behaviors exhibited by the system. **Section 4** includes the investigations and characterizations of the occurrence of extreme events. Ultimately, the conclusion is presented in **Section 5**.

2. Simplified Lorenz-like system

This section provides a review of the nonhyperbolic Lorenz-like chaotic system introduced by Kamdem Kuate et al.,[24] focusing on its major characteristics and dynamical features. The model is defined by the following system of differential equations (**System 1**):

$$\begin{cases} \dot{x}_1 = A\,(x_2 - x_1) \\ \dot{x}_2 = -x_1 \mathrm{sign}\,(x_3) \\ \dot{x}_3 = |x_2| - C \end{cases}$$

where $x_1, x_2,$ and x_3 are the three state variables, A and C are positive constant parameters. This mathematical model can be considered a highly simplified PWL version of the Lorenz system, a classic model for atmospheric convection and a benchmark for chaotic dynamics.[11]

The x_1-dynamics is structurally identical to its Lorenz counterpart. However, the other two equations are significantly simplified. The smooth quadratic nonlinearities of the Lorenz system $x_1 \cdot x_3$ and $x_1 \cdot x_2$ in the second and third equations are substituted with much simpler PWL terms: $x_1 \cdot \mathrm{sign}(x_3)$ and $|x^2|$, respectively. This modification makes **System (1)** more amenable to analytical study and significantly simplifies its electronic

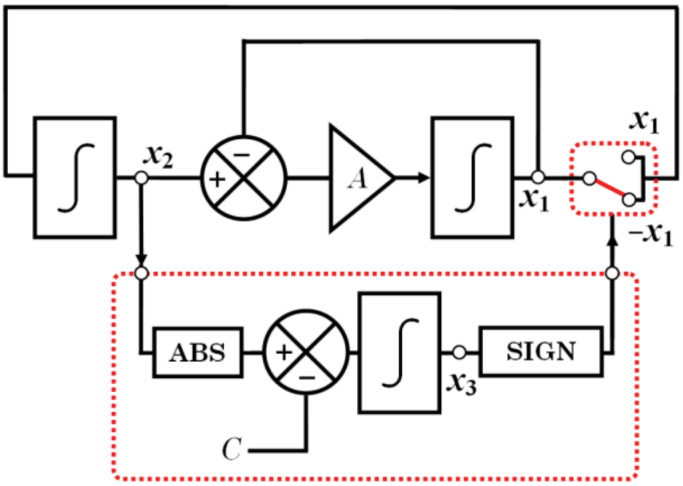

Figure 1. Block diagram of System 1

implementation, as multipliers are replaced by switches and rectifiers. As illustrated in Figure 1, the dynamics of the third state variable are derived from x_2, which introduces the system's nonlinearities and switching behavior.

The elegance of this model also lies in its amplitude control and offset boosting capabilities. The system's dynamics are mainly controlled by gain A, serving as the main bifurcation parameter. The constant C, on the other hand, acts as a convenient total amplitude controller. If the switching condition is changed from sign(x_3) to sign(x_3 + k), with $k \in \mathbb{R}$, the switching plane moves from x_3 = 0 to $x_3 = -k$. This shifts the entire attractor along the x_3-axis by $-k$, demonstrating an additional, simple degree of controllability in this model. The divergence of the flow for **System (1)** is computed as $\nabla F = -A$. The divergence is always negative, and the phase-space volume contracts exponentially over time, confirming the dissipative nature of the system. **System (1)** remains invariant under the transformation $(x_1, x_2, x_3) \to (-x_1, -x_2, x_3)$. This symmetry is associated with the coexistence of symmetric attractors. The derivation process of this system from the Lorenz equations, as well as its topological similarity with elegant Sprott-B and Sprott-C systems, is further explored by Kamdem Kuate et al.[24]

The dynamic behavior of nonlinear systems is closely related to the nature of equilibrium points. The occurrence of chaos and other complex dynamics can often be anticipated by analyzing the stability of these equilibria. The fixed points of **System (1)** are computed as $E^{\pm}(\pm C, \pm C, 0)$, both located on the $x_3 = 0$ plane and symmetrically placed with respect to the origin. The PWL nature of the system, particularly the sign term, makes standard linearization via the Jacobian matrix problematic. To circumvent this issue, the sign-nonlinearity is approximated by a hyperbolic tangent term tanh(nx), which is continuously differentiable. Here, n is a stiffness parameter chosen to facilitate the analytical study of the otherwise non-differentiable switching plane; n should be large enough to suitably fit the sign(x) function. Without loss of generality, n is set to 100. This leads to the equivalent smooth system in **System (2)**.

$$\begin{cases} \dot{x}_1 = A\,(x_2 - x_1) \\ \dot{x}_2 = -x_1 \tanh\,(n x_3) \\ \dot{x}_3 = |x_2| - C \end{cases} \tag{2}$$

The Jacobian matrix J of **System (2)** is computed at equilibrium points $E^{\pm}$ as follows Equation (3):

$$J^{\pm} = \begin{bmatrix} -A & A & 0 \\ 0 & 0 & \mp nC \\ 0 & \pm 1 & 0 \end{bmatrix} \tag{3}$$

The resulting characteristic equation is derived as Equation (4):

$$(\lambda + A)\left(\lambda^2 - nC\right) = 0 \tag{4}$$

This yields a negative real eigenvalue $\lambda_1 = -A$ and a purely imaginary complex conjugate pair $\lambda_{2,3} = \pm i\sqrt{nC}$, indicating the nonhyperbolic saddle-foci nature of equilibrium points $E^{\pm}$. The system's behavior near these points is oscillatory, but since the eigenvalues have zero real part, the linear approximation cannot definitively determine their stability. However, the presence of a negative real eigenvalue is characteristic of a stable manifold along one direction. As the system parameters are varied, these saddle-foci can become involved in the formation of a heteroclinic orbit, where a trajectory leaves one saddle point and approaches another, or a homoclinic orbit, where it returns to the same saddle point. These types of behaviors are well-known precursors to the onset of chaos and the formation of a strange attractor.

3. Dynamic analysis

This section presents an exhaustive numerical analysis of **System (1)** using standard tools, such as bifurcation diagrams, Lyapunov exponents (LEs), frequency spectra, phase portraits, and time series analyses. Diverse dynamic behaviors are investigated with a particular emphasis on bifurcations and amplitude control. **System (1)** was solved using fourth-order Runge–Kutta numerical methods for a time span ranging from 0 to 10^5 with a time-step $\Delta t = 0.001$. The transient regime over the interval 0–10^3 was systematically discarded from the generated time series. Bifurcation diagrams and LEs were respectively computed following the method described in Ali et al.[32] and Wolf's algorithm.[33] Combining these tools provides a comprehensive view of dynamics and highlights the transitions between chaotic and regular behaviors.

3.1. Effect of parameter A on dynamics

Figure 2 illustrates a bifurcation diagram of **System (1)** representing the local maxima of x_3 for increasing values of A, with C arbitrarily fixed at 2 and ICs (x_{10}, x_{20}, x_{30}) = $(\pm 1,\ 0,\ \pm 1)$. Only the two largest LEs are plotted, serving as critical indicators of system dynamics. Positive LE_1 is indicative of chaos, while $LE_1 \leq 0$ corresponds to regular behaviors (periodic or fixed point).

For $1 \leq A < 1.7$, the bifurcation diagram shows a dense and continuous distribution of maxima, indicating irregular oscillations covering a wide range of amplitudes. The LE spectrum confirms the dynamics' chaotic nature, with LE_1 consistently positive. The time series in this region appears unpredictable, with frequent random excursions to extremely large magnitudes. At $A \approx 1.7$, a boundary crisis occurs, and the chaotic attractor abruptly shrinks. Subsequently, the system undergoes a reverse period-doubling cascade, transitioning from chaos toward simpler periodic behaviors. The LE spectrum reflects this behavior, with LE_1 dropping to zero in these periodic windows. For $A \approx 1.76$, the system experiences an interior crisis leading to a larger chaotic attractor, which persists till A is approximately 1.95. As the parameter A exceeds 1.95, the attractor suddenly contracts, and the system undergoes a new cascade of reverse period-doubling bifurcations, progressively leading to periodic dynamics for $A > 2.06$. The system settles into a stable period-1 limit cycle characterized by $LE_1 = 0$. Figure 3 displays the phase portraits of **System (1)** projected on the x_1–x_3 plane for increasing values of A. The system displays coexisting symmetric attractors for $1.95 \leq A < 2.25$. Specifically, Figure 3E and F illustrates typical examples of coexisting chaotic attractors (Figure 3E, for $A = 2.05$) and coexisting period-2 limit-cycles (Figure 3F, for $A = 2.2$).

Figure 4 shows the evolution of the dynamic behavior of **System (1)** in both the time and frequency domains as parameter A increases. At $A = 1.6$ (Figure 4A and B), the system exhibits chaotic behavior, as evidenced by the broadband frequency spectrum and the irregular time-domain signal.

As A is increased to 1.75 (Figure 4C and D), the dynamics shift to a periodic state, characterized by sharp peaks (noticed at 0.08 and 0.15 Hz) and regular oscillations in the time domain. For A = 2 (Figure 4E and F), the system displays chaotic behavior, with a mixed-mode frequency spectrum and time-domain bursts. Ultimately, at A = 2.5 (Figure 4G and H), the system settles into a stable limit cycle, with a single dominant frequency of 0.125 Hz. These transitions highlight the system's sensitivity to changes in A, the primary control parameter.

To further substantiate the numerical analyses, the spectral features of **System (1)** are investigated using frequency spectra and parameter-dependent spectrograms.[34] These tools provide a comprehensive perspective on system dynamics, thereby bridging the gap between time-domain observations and underlying frequency-based mechanisms. The combination of the spectrogram and the evolution of dominant frequencies (f_{p1}, f_{p2}, and f_{p3}) of state variables (x_1, x_2, and x_3, respectively) in Figure 4 provides a clear representation of dynamical transitions occurring in **System (1)** as parameter A is varied. The spectrogram reveals a broad frequency distribution for A < 1.7, a signature of chaotic dynamics, which suddenly transitions to distinct frequency bands, indicating a shift toward more structured behavior.

Subsequently, the system exhibits another chaotic band located between 1.76 and 2.06, and progressively stabilizes into a periodic regime marked by a unique dominant frequency.

As demonstrated in Figure 5, the dominant frequencies of each state variable exhibit significant fluctuations for A < 1.7 and a sharp peak in f_{p3} at $A \approx 1.7$, aligning with the isolated periodic windows between 1.7 and 1.76. As A increases, x_3 shows higher frequencies compared to x_1 and x_2, which remain low and quite similar. This highlights the pivotal role of x_3 in driving the system's transition from chaos to order.

3.2. Effect of parameter C on dynamics

The bifurcation diagram and LEs in Figure 6 are plotted for increasing values of C, with A = 1.6. It reveals how this parameter modulates the magnitude and complexity of the system's dynamics while preserving its chaotic nature. For small values of C (from 0 to ~3), the system exhibits relatively low amplitudes. Its chaotic trajectory is confined to a smaller hypervolume around the origin.

As C increases, x_3 progressively displays larger local maxima, reflecting an expanded range and a greater variability. However, the largest LE_1 remains consistently positive with small fluctuations around 0.1, confirming the system's chaotic dynamics regardless of the value of C. This parameter acts as an amplitude controller, broadening the system's phase-space exploration while maintaining a consistent dynamic (fixed by A). Such a feature is relevant to engineered systems and represents a crucial asset in signal conditioning and integrated reprocessing.[34]

The spectral analyses of **System (1)** with respect to parameter C reveal a chaotic dynamic, evidenced by the broadband spectrogram in Figure 7. While x_1 and x_2 display relatively stable spectral distributions ($f_{p1,2} \approx 0.05$), x_3 shows significant changes in its power spectrum, accurately captured by the erratic variations of its dominant frequency, f_{p3}.

Figure 7B further underscores the pivotal role of x_3 in driving the system's irregularity through the PWL terms. The switching behavior induced by these nonlinearities introduces abrupt transitions and amplifies perturbations in the system dynamics, potentially leading to extreme events.

As a preliminary investigation, we computed the peak-to-peak magnitudes ($\Delta pp_{1,2,3}$) and the mean values of all three state variables as functions of parameter C (Figure 8).

The peak-to-peak magnitudes of all three state variables exhibit a monotonic increase as C varies from 0 to 10. The near-parallel trajectories of the three curves suggest a uniform scaling of all three state variables. Figure 8B illustrates a notable distinction in the mean values of state variables as C increases. While the mean values of x_1 and x_2 remain relatively constant, x_3 exhibits a significant shift to negative values, highlighting its unique sensitivity to changes in C. This feature directly results from the presence of C in the x_3-dynamics of **System (1)**, modulating the variations in x_3 and contributing to the dynamics of x_2 through the sign nonlinearity.

Figure 9 contrasts the dynamical behavior of **System (1)** for three values of parameter C and A = 2. C acts as a global amplitude controller and can be selectively tuned to adjust the attractor size. Smaller C values produce confined, orderly orbits, while larger values of C expand the trajectories, revealing amplified oscillations.

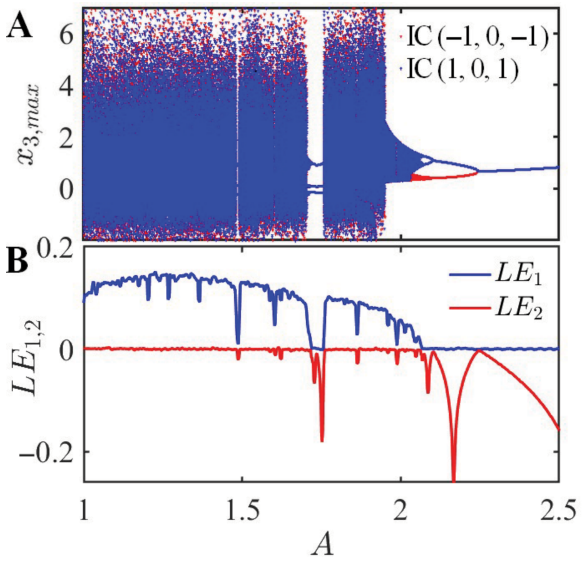

Figure 2. Dynamic behavior of the minimal Lorenz-like system. (A) Bifurcation diagram for increasing values of A. (B) The two largest LEs of **System (1)** computed for increasing values of parameter A. Other parameters are fixed as: $C = 2$ and (x_{10}, x_{20}, x_{30}) = $(\pm 1,\ 0,\ \pm 1)$.
Abbreviations: ICs: Initial conditions; LEs: Lyapunov exponents.

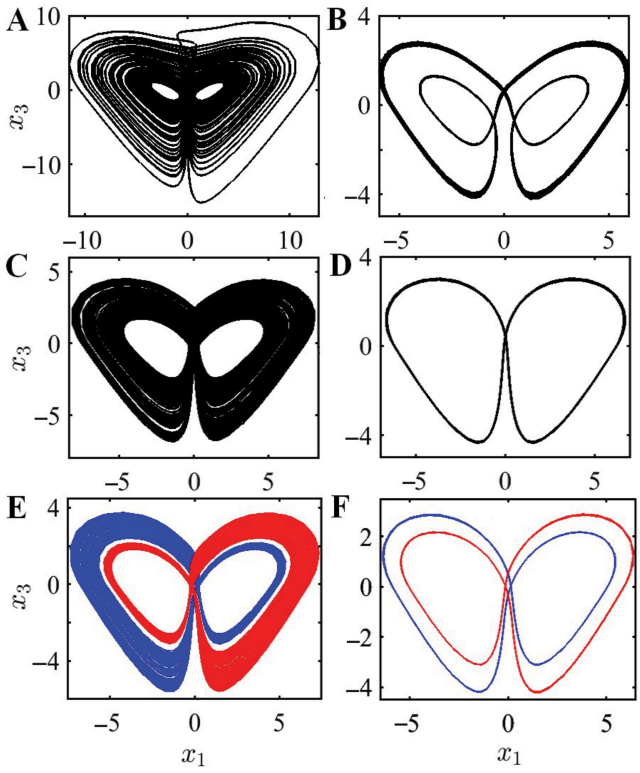

Figure 3. $x_1 - x_3$ phase portraits of **System (1)**. (A) $A = 1.6$. (B) $A = 1.75$. (C) $A = 2$. (D) $A = 2.5$. (E) $A = 2.05$. (F) $A = 2.2$. All with $C = 2$ and (x_{10}, x_{20}, x_{30}) = $(\pm 1,\ 0,\ \pm 1)$.

4. Characterization of extreme events

The analysis of extreme events in dynamic systems is crucial for understanding how minor changes in parameters can lead to significant shifts in behavior, often resulting in unpredictable, high-amplitude fluctuations. Notwithstanding its simplicity, **System (1)** displays a propensity to generate high-amplitude signals, especially for small values of parameter A. The aim of this section is to investigate and characterize such dynamics through statistical analyses. The local maxima of variable x_1 are arbitrarily designated as events in the time course of the system. Within this framework, extreme events are delineated as local maxima exceeding the significant height threshold, which is defined as follows Equation (5):

$$H = \mu + d\sigma \tag{5}$$

where μ is the average value of all local maxima recorded for a long numerical run; σ is the standard deviation of

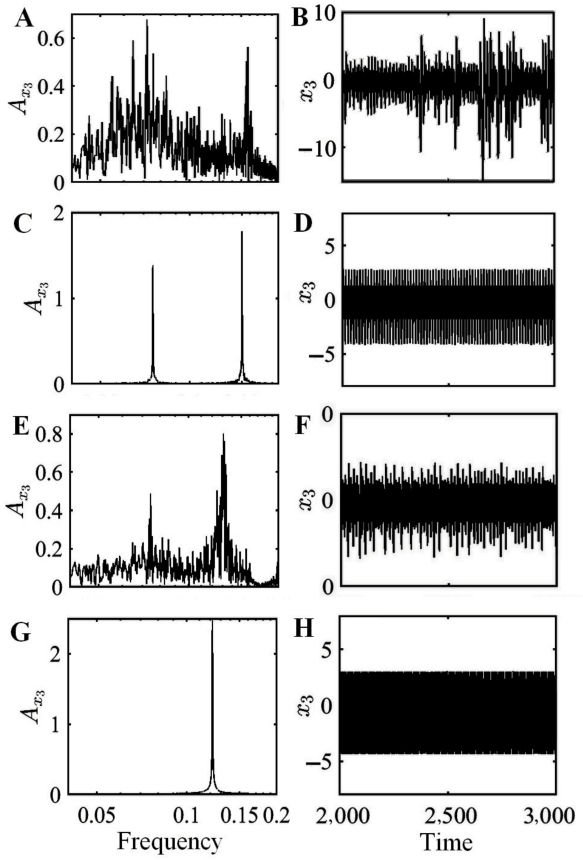

Figure 4. Frequency spectrum (left) and corresponding time series (right) of **System (1)**. (A, B) $A = 1.6$. (C, D) $A = 1.75$. (E, F) $A = 2$. (G, H) $A = 2.5$. All with $C = 2$ and $(x_{10}, x_{20}, x_{30}) = (1,\ 0,\ 1)$.

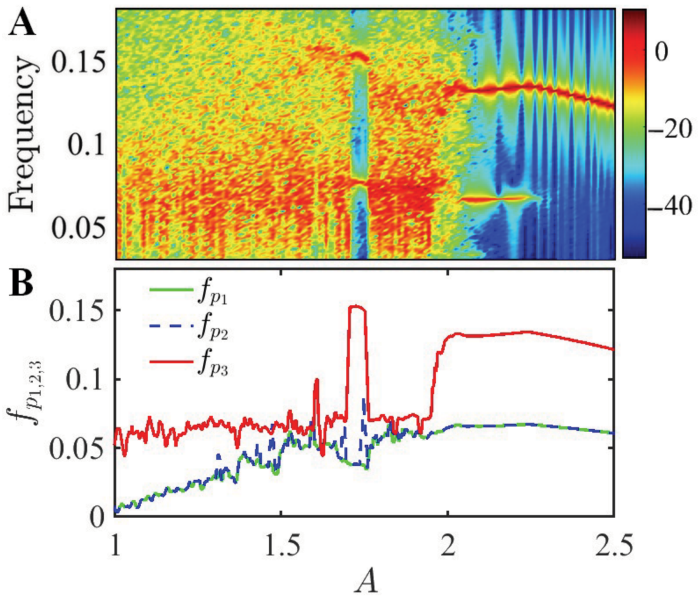

Figure 5. Spectral dynamics of the minimal Lorenz-like system. (A) Parameter-dependent spectrogram of **System (1)**. (B) Evolution of dominant frequencies as the parameter A is varied. $C = 2$ and $(x_{10}, x_{20}, x_{30}) = (1,\ 0,\ 1)$.

these local maxima; and d, generally selected between 4 and 8, is an arbitrarily chosen coefficient determining the extent to which the observed event is shifted from the nominal dynamics of the system.[35,36] A low value of d will include nominal fluctuations, failing to isolate extreme events, while an excessively high value of d will result in a sample size too small for statistical validity. The threshold H is chosen based on the system's dynamical properties and, therefore, depends on the specific system under consideration. In the present study, we assume d = 5.5 as this value provides an optimal balance for sufficiently isolating the outlier events from the nominal

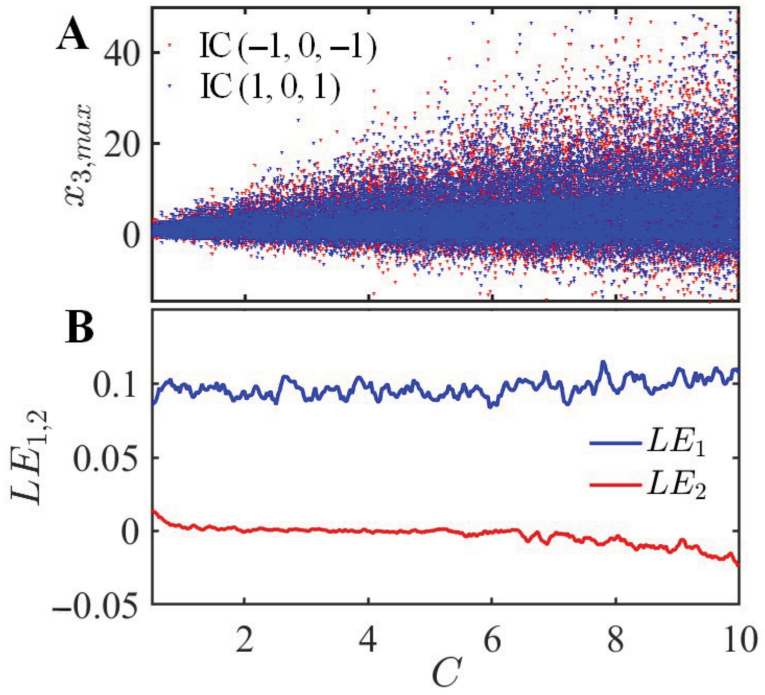

Figure 6. Dynamic behavior of the minimal Lorenz-like system. (A) Bifurcation diagram for increasing values of C. (B) The two largest Lyapunov exponents (LEs) of **System (1)** computed for increasing values of parameter C. Other parameters are fixed as: $A = 1.6$ and initial conditions (ICs) $(x_{10}, x_{20}, x_{30}) = (\pm 1,\ 0,\ \pm 1)$.

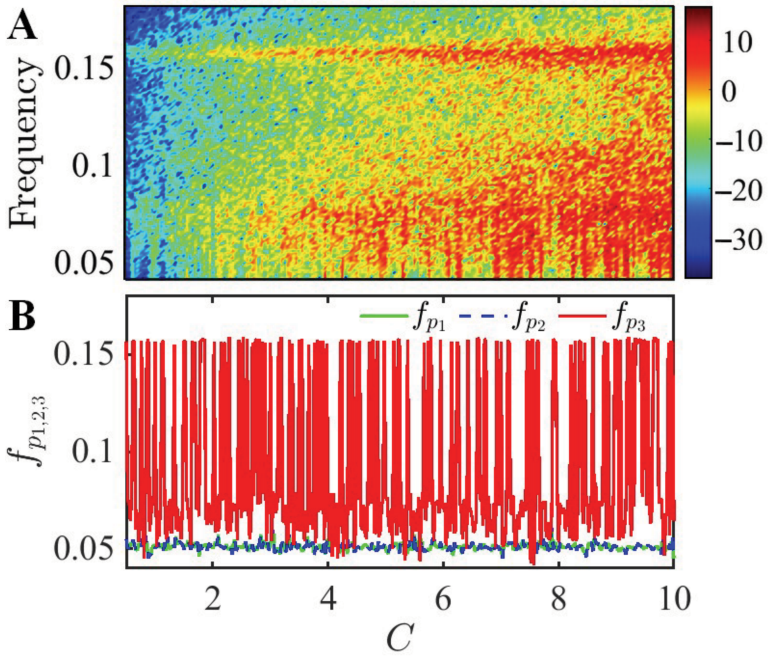

Figure 7. Spectral dynamics of the minimal Lorenz-like system. (A) Parameter-dependent spectrogram of**System (1)**. (B) Evolution of dominant frequencies as the parameter C is varied. $A = 1.6$ and $(x_{10}, x_{20}, x_{30}) = (1,\ 0,\ 1)$.

dynamics while retaining enough data points. However, it is important to note that extreme events can also be observed for other values of d.

4.1. Parametric setting

For d = 5.5, C = 2, and (x_{10}, x_{20}, x_{30}) = (1, 0, 1), long-run simulations were carried out for increasing values of A, and local maxima were systematically recorded. The obtained data are used to construct the parameter-dependent bifurcation diagram in Figure 10A. Local maxima of x_1 that exceed the threshold value are identified as extreme events. Such occurrences are consistently observed for smaller values of A. As this parameter is increased, these events progressively become part of the nominal dynamics. This is further illustrated in Figure 10B, which shows the distribution of extreme events across different regions of the A–C parametric space. Given that C exerts no significant effect on the system's qualitative dynamic

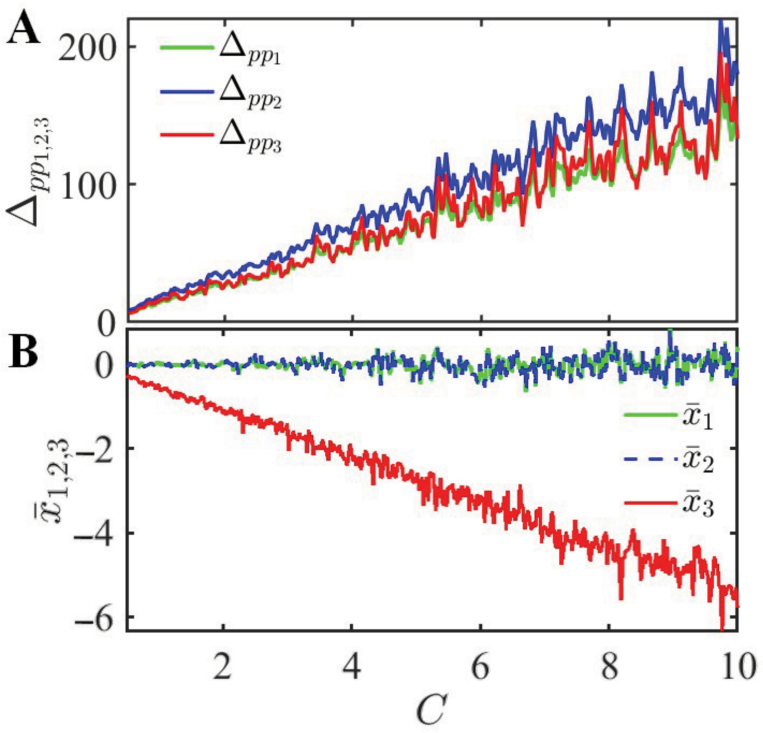

Figure 8. Amplitude control of the minimal Lorenz-like system. (A) Peak-to-peak values of state variables. (B) Average values of state variables for increasing values of parameter C. With $A = 1.6$ and (x_{10}, x_{20}, x_{30}) = (1, 0, 1).

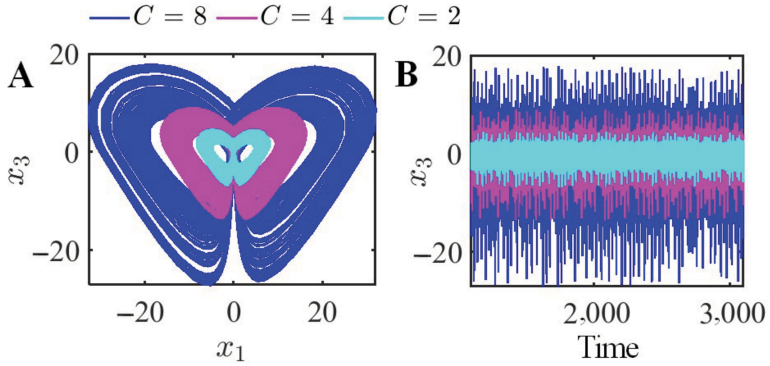

Figure 9. Parametric control of attractor size. (A) $x_1 - x_3$ phase portraits of **System (1)**. (B) corresponding time series, plotted with $A = 2$ and (x_{10}, x_{20}, x_{30}) = (1, 0, 1).

behavior, the same trend is observed across almost all values of this parameter. When $A \approx 1$, the system displays complex patterns in the time series and seemingly random occurrences of high magnitudes across all state variables, particularly x_1. As the parameter A increases, the system tends to exhibit a moderate, confined dynamic behavior.

Figure 11 illustrates the identification and separation of extreme events in phase space and time domains for two discrete values of A. For A = 1.96, the phase portrait reveals a compact chaotic attractor confined in a specific region of phase space. Although chaotic, the system's trajectory revisits neighboring states. The corresponding time series further supports this observation, as the variable x_1 fluctuates within a limited range, rarely exceeding the threshold.

In contrast, for A = 1, the system generates a complex attractor structure, thereby demonstrating an expanded trajectory across the phase space. The related time series corroborates this, showing frequent and significant excursions beyond the threshold for extreme events. This is further substantiated by the PoincarÃ© map and the first return map of local maxima plotted for the same set of parameters and ICs.

The Poincaré maps in Figure 12A and B offer a granular perspective on the system's behavior by capturing the intersections of the system trajectory with a defined plane (x_3 = 0). Isolated points deviating from the nominal dynamics and crossing the PoincarÃ© section above the extreme-event threshold are observed for A = 1. This dispersion suggests a broader exploration of phase space, consistent with the expanded phase portrait and frequent threshold crossings in the time series. The first return maps in Figure 12C and D provide further insights into the evolution of extreme events by illustrating the relationship between successive maxima of x_1. The nominal dynamics exhibit a dense clustering of points near the origin, with a limited number of points scattered along the diagonal and below the

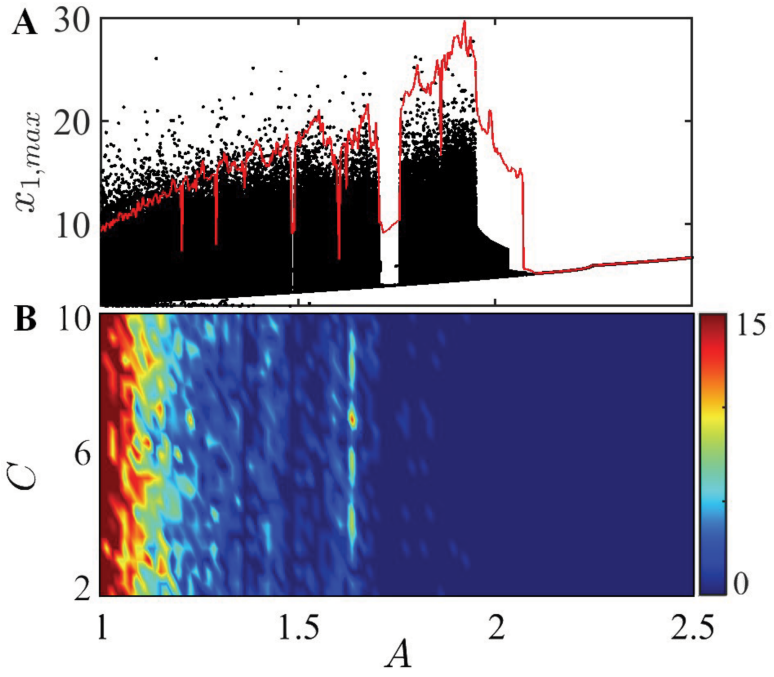

Figure 10. Extreme events map in the $A - C$ parametric plane. (A) Bifurcation diagram of **System (1)** showing the occurrence of extreme events for increasing values of A and $C = 2$. (B) Two-dimensional parametric map of extreme events.

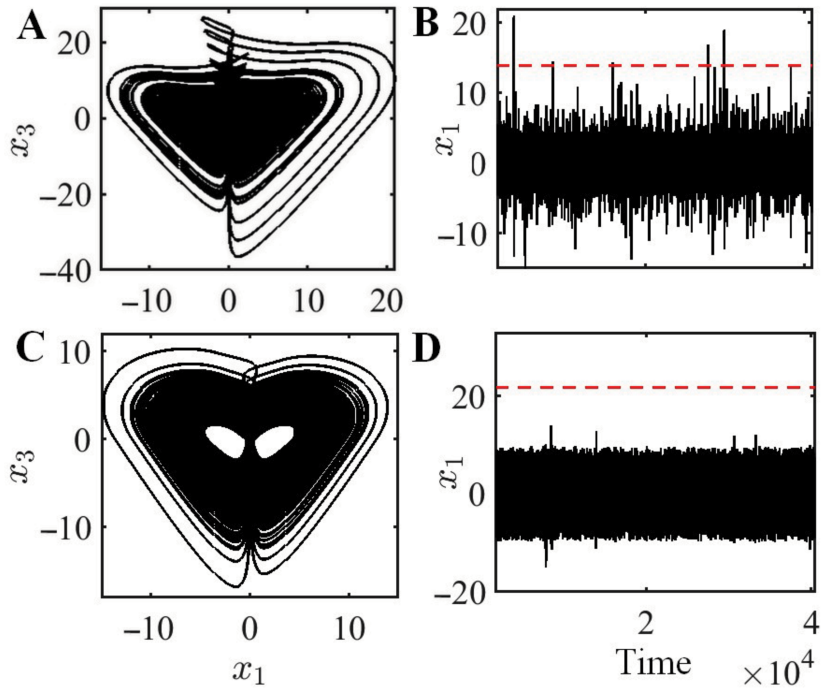

Figure 11. Identification of extreme events in phase-space and time-domain. (A, B) $x_1 - x_3$ phase portraits and time series of **System (1)** for $A = 1$. (C, D) $x_1 - x_3$ phase portraits and time series for $A = 1.96$. All plotted for $C = 2$ and $(x_{10}, x_{20}, x_{30}) = (1,\ 0,\ 1)$.

threshold. Conversely, a broader distribution with clusters forming away from the origin and extending toward higher values of $x_{1,\text{max}}$ is indicative of the occurrence of extreme events.

4.2. Statistical characterization of extreme events

Extreme events are fundamentally defined by their high magnitude and their rarity.[34] It is imperative that these two properties are investigated to achieve a comprehensive characterization of the dynamics present in **System (1)**. This is achieved by estimating the probability density function (PDF) of event height.

Figure 13 presents the PDF of the local maxima of the variable x_1, offering a statistical perspective on the distinction and identification of extreme events.[37] For A = 1.96 (Figure 13A), the distribution displays peaks around 0.35 and 5.00, indicating that most peak values cluster near these magnitudes. The gradual decline observed on the right-hand side for increasing $x_{1,\text{max}}$ reflects the smaller probabilities for higher magnitudes. However, no

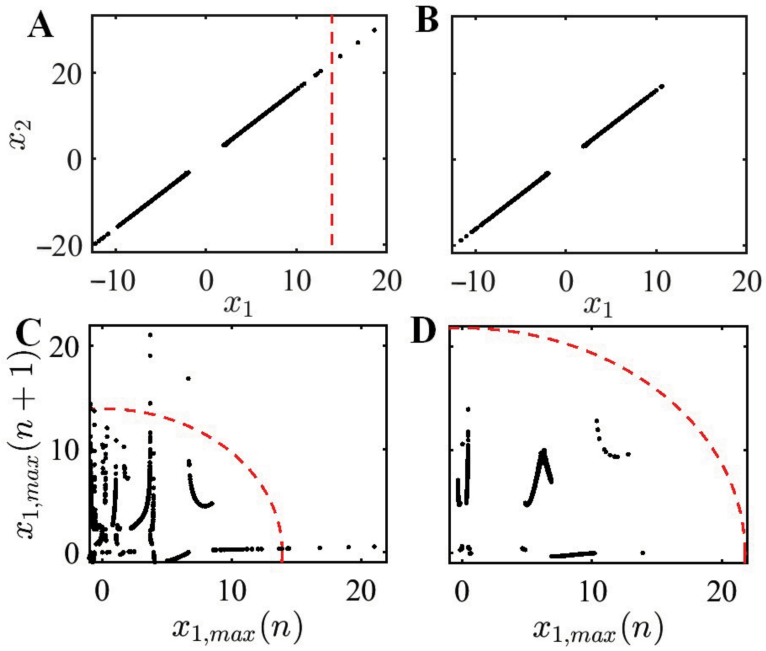

Figure 12. Poincaré map ($x_3 = 0$) and first return map of local maxima. (A, B) $A = 1$. (C, D) $A = 1.96$. All $C = 2$, (x_{10}, x_{20}, x_{30}) = (1, 0, 1).

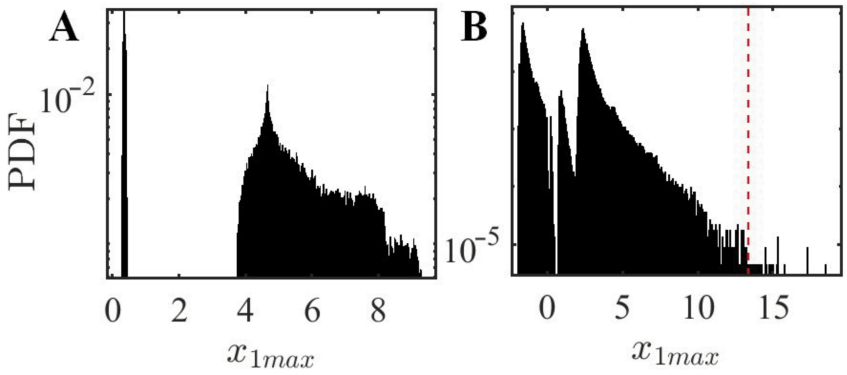

Figure 13. Probability density function (PDF) of local maxima of **System (1)**. (A) $A = 1.96$. (B) $A = 1$. Both $C = 2$.

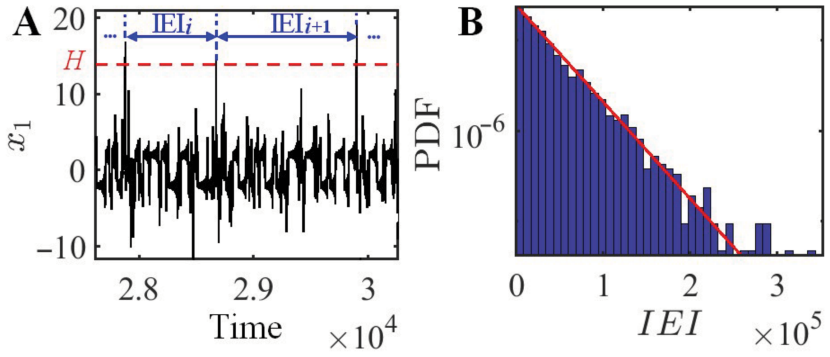

Figure 14. Characterization of rarity of extreme events in the time-domain. (A) Illustration of inter-event intervals (IEI). (B) Probability density function (PDF) distribution of these IEI, for $A = 1$ and $C = 2$.

extreme events are observed for this parameter setting. The PDF in Figure 13B, plotted for A = 1, shows a heavy-tailed distribution, with a high probability density for smaller values of $x_{1,\max}$, and a gradual decay as $x_{1,\max}$ increases, with the majority of local maxima concentrated at lower values. A non-negligible probability of observing significantly larger values, indicative of extreme events, is observed. This is further substantiated by the presence of a long tail extending beyond the threshold. Even though such events are relatively rare, their occurrence

is statistically significant, as evidenced by the non-zero probability density in the tail region. To further characterize such dynamic behavior, it is necessary to estimate the return time between successive extreme events. The probability distribution of inter-event intervals (IEIs) determined for a substantial numerical run of the system enables the comprehensive delineation of the exhibited dynamics and the confirmation of the existence of extreme events in **System (1)**.

The PDF of IEIs in Figure 14 shows a broad distribution with many short intervals and a non-negligible probability of long intervals. This behavior is consistent with statistics of rare, weakly correlated events and can be approximated by an exponential (Poisson-process) distribution. The PDF is then fitted by Equation (6):

$$P(r) = \lambda e^{-\lambda r} \tag{6}$$

where r denotes the IEI and λ is the rate parameter whose estimated value is $\lambda \sim 2.46 \times 10^{-5}$.

5. Conclusion

The present study has provided a comprehensive analysis of a minimal Lorenz-like system featuring only PWL nonlinearities, focusing on its dynamical complexity and the emergence of extreme events. The parametric analysis of the system has been conducted using bifurcation diagrams, LEs, and statistical tools. It has been demonstrated that a unique control parameter governs the system dynamics and the transitions between chaotic, periodic, and extreme-event regimes. The heavy-tailed distribution of IEIs has further elucidated the system's ability to exhibit rare, high-amplitude fluctuations. The findings highlight the system's potential as a simplified yet powerful model for studying extreme events. Subsequent studies in this framework should explore the predictability of such events using machine learning algorithms or multi-agent systems,[38,39] as well as provide experimental validation of such intricate behavior.

Acknowledgments

None.

Funding

None.

Conflict of interest

Paul Didier Kamdem Kuate is an Editorial Board Member of this journal, but was not in any way involved in the editorial and peer-review process conducted for this paper, directly or indirectly. Separately, other authors declared that they have no known competing financial interests or personal relationships that could have influenced the work reported in this paper.

Author contributions

Conceptualization: Jianning Huang, Paul Didier Kamdem Kuate
Investigation: Jianning Huang, Achille Ecladore Tchahou Tchendjeu
Methodology: Jianning Huang, Achille Ecladore Tchahou Tchendjeu
Writing–original draft: Jianning Huang
Writing – review & editing: Jianning Huang, Paul Didier Kamdem Kuate

Availability of data

The numerical datasets and simulation codes generated and analyzed during the current study are available from the corresponding author on reasonable request.

AI Tools Statement

All authors confirm that no AI tools were used in the preparation of this manuscript.

References

1. Durairaj P, Kanagaraj S, Kumarasamy S, and Rajagopal K. Emergence of extreme events in a quasiperiodic oscillator. *Phys Rev E.* 2023;107(2):L022201. https://doi.org/10.1103/PhysRevE.107.L022201
2. Stewart M, Carleton WC, Groucutt HS. Extreme events in biological, societal, and earth sciences: a systematic review of the literature. *Front Earth Sci.* 2022;10:786829. https://doi.org/10.3389/feart.2022.786829
3. Alvre J, Broska LH, Rübbelke DTG. Studying extreme events: an interdisciplinary review of recent research. *Heliyon.* 2024;10(24):e41024. https://doi.org/10.1016/j.heliyon.2024.e41024
4. Broska LH, Poganietz W-R, Vögele S. Extreme events defined—a conceptual discussion applying a complex systems approach. *Futures.* 2020;115:102490. https://doi.org/10.1016/j.futures.2019.102490
5. Zhou X, Li Y, Xiao C, Chen W, Mei M, Wang G. High-impact extreme weather and climate events in China: summer 2024 overview. *Adv Atmos Sci.* 2025;42(6):1064-1076. https://doi.org/10.1007/s00376-024-4462-6
6. Zhao D, Li Y, Xu Y, Liu Q, and Kurths J. Extreme events in a class of nonlinear Duffing-type oscillators with a parametric periodic force. *Eur Phys J Plus.* 2022;137:314. https://doi.org/10.1140/epjp/s13360-022-02530-z
7. Diffenbaugh NS, Pal JS, Trapp RJ, and Giorgi F. Fine-scale processes regulate the response of extreme events to global climate change. *Proc Natl Acad Sci U S A.* 2005;102(44):15774-15778. https://doi.org/10.1073/pnas.0506042102
8. Penduff T, Sérazin G, Leroux S, et al. Chaotic variability of ocean heat content: Climate-relevant features and observational implications. *Oceanography.* 2018;31(2):63-71. https://doi.org/10.5670/oceanog.2018.210
9. Sura P, Sardeshmukh PD. Reconciling non-Gaussian climate statistics with linear dynamics. *J Climate.* 2008;21(22):5962-5983. https://doi.org/10.1175/2008JCLI2358.1
10. Sale M, Mohammad RG, Amin F. Nonlinear dynamic modeling and chaos analysis of aircraft landing gear under two- and three-point landings. *Nonlinear Sci Control Eng.* 2025;1(1):025280001. https://doi.org/10.36922/NSCE025280001
11. Lorenz EN. Deterministic nonperiodic flow. *J Atmos Sci.* 1963;20(2):130-141. https://doi.org/10.1175/1520-0469(1963)020%3C0130:DNF%3E2.0.CO;2
12. Lorenz EN. *The Essence of Chaos.* University of Washington Press; 1993.
13. Strogatz SH. *Nonlinear Dynamics and Chaos: With Applications to Physics, Biology, Chemistry, and Engineering.* 2nd ed. Westview Press; 2015.
14. Palmer TN. The primacy of doubly stochastic models for climate prediction. *Proc Natl Acad Sci U S A.* 2019;116(23):11195-11200. https://doi.org/10.1016/B978-0-12-473750-1.50009-6
15. Sun KH, Sprott JC. Dynamics of a simplified Lorenz system. *Int J Bifurcation Chaos.* 2009;19(4):1357-1366. https://doi.org/10.1142/S0218127409023688
16. Liu Y, Yang Q. Dynamics of a new Lorenz-like chaotic system. *Nonlinear Anal Real World Appl.* 2010;11(4):2563-2572. https://doi.org/10.1016/j.nonrwa.2009.09.001

17. Letellier C, Mendes EMAM, Malasoma J-M. Lorenz-like systems and Lorenz-like attractors: definition, examples, and equivalences. *Phys Rev E.* 2023;108(4):044209. https://doi.org/10.1103/PhysRevE.108.044209
18. van der Schrier G, Maas LRM. The diffusionless Lorenz equations; Shil'nikov bifurcations and reduction to an explicit map. *Physica D.* 2000;141(1):19-36. https://doi.org/10.1016/S0167-2789(00)00033-6
19. Dong C-W. Periodic orbits of diffusionless Lorenz system. *Acta Phys Sin.* 2018; 67(24):240501. https://doi.org/10.7498/aps.67.20181581
20. Sprott JC. Some simple chaotic flows. *Phys Rev E.* 1994;50(2):R647. https://doi.org/10.1103/PhysRevE.50.R647
21. Sprott JC. Simple chaotic systems and circuits. *Am J Phys.* 2000;68(8):758-763. https://doi.org/10.1119/1.19538
22. Sprott JC. *Elegant Chaos: Algebraically Simple Chaotic Flows.* World Scientific; 2010.
23. Verhulst F, Bakri T. The Sprott B system. *Chaos.* 2024;34(10):103116. https://doi.org/10.1063/5.0212565
24. Kamdem Kuate PD, Lai Q, Fotsin H. Dynamics, synchronization and electronic implementations of a new Lorenz-like chaotic system with nonhyperbolic equilibria. *Int J Bifurcation Chaos.* 2019;29(14):1950197. https://doi.org/10.1142/S0218127419501979
25. Campos-Cantón E, Barajas-Ramírez JG, Solis-Perales G, Femat R. Multiscroll attractors by switching systems. *Chaos.* 2010;20(1):013116. https://doi.org/10.1063/1.3314278
26. Escalante-González RJ, Campos-Cantón E. Generation of multiscroll attractors without equilibria via piecewise linear systems. *Chaos.* 2017;27(5):053109. https://doi.org/10.1063/1.4983523
27. Wang N, Sun K, Sprott JC. Generating multi-scroll Chua's attractors via simplified piecewise-linear Chua's diode. *IEEE Trans Circuits Syst I Regul Pap.* 2019;94(12):125203. https://doi.org/10.1109/TCSI.2019.2933365
28. Kuate PD, Tchahou Tchendjeu AE, Fotsin H. A modified Rössler prototype-4 system based on Chua's diode nonlinearity: dynamics, multistability, multiscroll generation and FPGA implementation. *Chaos Solitons Fractals.* 2020;140:110213. https://doi.org/10.1016/j.chaos.2020.110213
29. Campos-Cantón E, Femat R, Chen G. Attractors generated from switching unstable dissipative systems. *Chaos.* 2012;22(1):013121. https://doi.org/10.1063/1.4742338
30. Escalante-González RJ, Nicol M. A monoparametric family of piecewise linear systems to generate scroll attractors via path-connected set of polynomials. *Int J Bifurcation Chaos.* 2017;27(13):1750040. https://doi.org/10.1142/S0218127421500346
31. Li C, Sprott JC. Coexisting hidden attractors in a 4D simplified Lorenz system. *Int J Bifurcation Chaos.* 2014;24(12):1450034. https://doi.org/10.1142/S0218127414500345
32. Ali J, Iqtadar H, Fahimeh N, Seyed Mohammad RHG, Sajad J. A simple guide for plotting a proper bifurcation diagram. *Int J Bifurcation Chaos.* 2021;31(01):2150011. https://doi.org/10.1142/S0218127421500115
33. Wolf A, Swift JB, Swinney HL, Vastano JA. Determining Lyapunov exponents from a time series. *Physica D.* 1985;16(3):285-317. https://doi.org/10.1016/0167-2789(85)90011-9
34. Wan Z, Pu Y-F, Lai Q. Memristive feedback-controlled chaotic system with diverse dynamics. *Nonlinear Sci Control Eng.* 2025;1(1):025310008. https://doi.org/10.36922/NSCE025310008
35. Ray A, Mishra A, Ghosh D, Kapitaniak T, Dana SK, Hens C. Extreme events in a network of heterogeneous Josephson junctions. *Phys Rev E.* 2020;101(3):032209. https://doi.org/10.1103/PhysRevE.101.032209
36. Malik N, Ozturk U. Rare events in complex systems: understanding and prediction. *Chaos.* 2020;30(9):090401. https://doi.org/10.1063/5.0024145
37. Ahmadi A, Parthasarathy S, Pal N, Rajagopal K, Jafari S, Tlelo-Cuautle E. Extreme multistability and extreme events in a novel chaotic circuit with hidden attractors. *Int J Bifurcation Chaos.* 2023;33(7):2330016. https://doi.org/10.1142/S0218127423300161
38. Rao H, Zhao Y, Chen H-P. Predicting chaotic system behavior using machine learning techniques. *Nonlinear Sci Control Eng.* 2025;1(1):025290003. https://doi.org/10.36922/NSCE025290003
39. Wang J-Y, Zhao X-W, Pang D, Liu Z-W. Predefined-time practical containment control for multi-agent systems via event-triggered control. *Nonlinear Sci Control Eng.* 2025;1(1):025290002. https://doi.org/10.36922/NSCE025290002